RESEARCH PAPER

Fe₃O₄-Polyvinylpyrrolidone-Decorated on Graphene Oxide Nanosheets for Fast Detection of Trace Protein

Dildora Mengliyeva ^{1*}, Marhaboxon Shomaqsudova ², Dilfuza Mirzaeva ³, Akmaljon Okboev ⁴, Khalima Aripova ⁵, Isroil Jumayev ⁶, Guljamol Makhmudova ⁷, Narzullaeva Oygul ¹, Tulkin Kadirov ⁸, Negmurod Rashidov ⁹, Nurbek Radjabov ¹, Otabek Mirzayev ¹⁰, Abduraimova Maftunakhan Akhmatovna ¹¹

- ¹ Bukhara State Medical Institute named after Abu Ali ibn Sino, Bukhara, Uzbekistan
- ² Alfraganus University, Tashkent, Uzbekistan
- ³ Tashkent State Medical University, Tashkent, Uzbekistan
- ⁴ Tashkent Institute of Irrigation and Agricultural Mechanization Engineers National Research University, Tashkent, Uzbekistan
- ⁵ Bukhara State Pedagogical Institute, Bukhara, Uzbekistan
- ⁶ Chirchik State Pedagogical University, Chirchik, Uzbekistan
- ⁷ Bukhara State Medical Institute, Bukhara, Uzbekistan
- ⁸ Samarkand Regional Center for Pedagogical Skills, Samarkand, Uzbekistan
- ⁹ Bukhara State University, Bukhara, Uzbekistan
- ¹⁰ Urgench State University named after Abu Rayhan Beruni, Urgench, Uzbekistan
- ¹¹ Tashkent State University of Economics, Tashkent, Uzbekistan

ARTICLE INFO

Article History:

Received 28 June 2025 Accepted 25 September 2025 Published 01 October 2025

Keywords:

Detection of protein Graphene oxide Fe_3O_4 PVPTrace protein

ABSTRACT

We reported a magnetically recoverable Fe₃O₄-PVP-GO nanocomposite designed for rapid, selective detection of trace proteins in complex matrices, addressing the persistent challenges of capture specificity, enrichment without dilution, and low-cost readout in point-of-care settings. The synthesis integrates three components: Fe₃O₄ magnetic cores for fast, quantitative magnetic separation; polyvinylpyrrolidone (PVP) to stabilize and present a hydrophobic/ hydrogen-bonding interface; and graphene oxide (GO) to provide a highsurface-area scaffold with abundant π – π and electrostatic interaction sites. The resulting Fe₂O₄-PVP-GO nanocomposite achieves near-quantitative recovery (>99.5%) within 30 seconds under a modest magnetic field (1.2 T), enabling rapid preconcentration from 10 mL samples and minimizing matrix carryover. Characterization by FE-SEM, FT-IR, XRD, VSM, and TGA confirms preserved magnetite crystallinity, substantial surface area, and robust integration of components without covalent grafting, indicating a predominantly supramolecular assembly driven by π - π interactions and hydrogen bonding. Binding to model trace proteins (BSA) demonstrated sub-attomolar detection limits (LOD ≈ 0.45 fM) with a three-log dynamic range (0.1–100 ng mL⁻¹) and inter-day RSD ≤ 3.9%. Real-sample analyses in human serum, skimmed milk, and river water yielded recoveries of 93-104% with minimal matrix effects. Reusability over fifteen cycles showed <4% loss in binding capacity. This work establishes a robust, low-cost platform for rapid on-site protein quantification with high fidelity and scalability.

How to cite this article

Mengliyeva D., Shomaqsudova M., Mirzaeva D. et al. Fe_3O_4 -Polyvinylpyrrolidone-Decorated on Graphene Oxide Nanosheets for Fast Detection of Trace Protein . J Nanostruct, 2025; 15(4):2071-2083. DOI: 10.22052/JNS.2025.04.047

^{*} Corresponding Author Email: remahahassan@hotmail.com

INTRODUCTION

Protein detection has travelled a remarkable arc since the first colorimetric biuret assay was introduced in 1887, yet the pursuit of everlower limits remains as urgent as ever [1-4]. From early clinical diagnostics that wrestled milligrams of albumin out of urine, the field has been driven by the realization that femtomolar fluctuations in cytokines, cardiac troponins, or circulating oncoproteins can herald disease months before overt symptoms appear. This historical compression from macro to micro to single-molecule sensitivity has repeatedly redrawn the boundaries of analytical chemistry, but it has also exposed a stubborn paradox: the more exquisite the detection, the more fragile the signal becomes against a background of salts, lipids, and myriad competing macromolecules [5-7]. Trace proteins, often present at concentrations five to six orders of magnitude below albumin, are particularly vulnerable to nonspecific adsorption, conformational masking, and stochastic loss at interfaces, turning each dilute sample into a kinetic battleground where picograms can be gained or forfeited in seconds [8, 9]. Consequently, modern assays must reconcile three seemingly incompatible imperatives: capture with absolute specificity, enrichment without dilution, and read-out with portable, low-cost instrumentation. These challenges have catalyzed a renaissance of nanomaterial design, yet the question persists: how can a single platform offer both the avidity of an antibody and the speed of a smartphone sensor without succumbing to the tyranny of background noise that has haunted trace protein analysis since its inception [10-12].

Recent studies (2020-2024) have harnessed an expanding menagerie of nanoparticles to push protein detection into the sub-femtomolar regime. Gold nanoclusters capped with zwitterionic peptides now enable single-digit pg mL⁻¹ quantification of cardiac troponin I by plasmonenhanced fluorescence, while silica-coated upconversion nanoparticles conjugated to aptamers report interleukin-6 in serum down to 0.8 fg mL⁻¹ via time-gated luminescence [13-15]. Carbon-based hybrids graphene quantum dots decorated with molecularly imprinted polymers have selectively enriched prostate-specific antigen at 50 aM in whole blood, and magnetic Fe₃O₄@polydopamine nanospheres integrated into microfluidic chips deliver 5-min on-chip pre-concentration of cytokines prior to electrochemical read-out [16-18]. Beyond inorganic cores, self-assembled protein nanoparticles (recombinant human serum albumin cross-linked with glutaraldehyde) are emerging as biodegradable carriers that co-load horseradish peroxidase for signal amplification, achieving 10 aM sensitivity for SARS-CoV-2 spike protein in saliva [19, 20]. Notably, hybrid nanozymes Fe₃O₄ nanocrystals embedded in bovine serum albumin cages marry peroxidase-like activity with magnetic separation to quantify trace ferritin at 2.3 aM in cerebrospinal fluid within 8 min. These vignettes illustrate a convergent trend: by marrying high-surface-area nanomaterials with affinity ligands or catalytic centres, researchers are routinely breaching the zeptomolar wall while retaining operational simplicity compatible with point-of-care deployment.

Yet, the very features that grant such exquisite sensitivity also seed their principal disadvantages. Gold and silica platforms necessitate complex surface chemistries whose batch-to-batch reproducibility remains problematic; a 15 % variation in aptamer density can shift the limit of detection by an order of magnitude [21-23]. Up-conversion nanoparticles, while photostable, demand 980 nm excitation that risks local heating and denaturation of fragile proteins. Carbonaceous hybrids suffer from irreversible fouling in whole-blood matrices, requiring sacrificial antifouling layers that lengthen assay time and increase cost. Magnetic cores, although enabling rapid separation, are prone to oxidative dissolution in acidic media (pH < 5), releasing Fe2+/ Fe³⁺ ions that catalyze Fenton-type degradation of the target protein a concern especially when quantifying oxidatively labile biomarkers such as Aβ oligomers. Protein-based nanocarriers mitigate cytotoxicity but introduce immunogenicity risks and potential prion transmission when animalderived proteins are employed. Finally, virtually all current platforms rely on high-affinity capture ligands (antibodies, aptamers, MIPs) whose shelf life rarely exceeds six months at 4 °C, thereby constraining large-scale deployment in resourcelimited settings. Addressing these limitations particularly oxidative stability, batch consistency, and ligand longevity remains the critical hurdle before nanomaterial-enabled trace protein diagnostics can transition from elegant laboratory curiosities to robust environmental or clinical workhorses [24-28].

Hence, the present study was conceived to design and validate a magnetically recoverable Fe_3O_4 —polyvinylpyrrolidone graphene oxide nanocomposite capable of selectively capturing and rapidly quantifying trace proteins in complex matrices at sub-attomolar abundance, thereby bridging the persistent gap between analytical sensitivity and real-world applicability.

MATERIALS AND METHODS

General remarks

All reagents were of analytical grade or higher and employed without further purification unless otherwise stated. Graphite flakes (99.9 %, 325 mesh) were purchased from Alfa Aesar; potassium permanganate (ACS, ≥ 99 %), sulfuric acid (98 %), hydrochloric acid (37 %), hydrogen peroxide (30 % w/w), iron (II) sulfate heptahydrate (≥ 99 %), iron (III) chloride hexahydrate (≥ 98 %), ammonium hydroxide (25 % NH₃), and polyvinylpyrrolidone (PVP, Mw \approx 40 kDa) were obtained from Merck. Sodium nitrate, N,N-dimethylformamide (HPLC grade), ethanol (absolute), and de-ionised water (18.2 $M\Omega$ cm, produced by a Milli-Q Integral system) were used throughout. Bovine serum albumin (BSA, lyophilised, ≥ 98 %) served as the model trace protein for all detection experiments. Characterization was performed with the following instruments. Field-emission scanning electron microscopy (FE-SEM) images were acquired on a JEOL JSM-7610F microscope operated at 5 kV; samples were sputter-coated with a 5 nm Pt layer to mitigate charging. Fourier-transform infrared (FT-IR) spectra were recorded on a Bruker Vertex 70 spectrometer equipped with a diamond ATR accessory, scanning from 4000 to 400 cm⁻¹ at 4 cm⁻¹ resolution and 32 accumulations. Powder X-ray diffraction (XRD) patterns were collected on a PANalytical Empyrean diffractometer using Cu $K\alpha$ radiation (λ = 1.5406 Å) over the 2θ range 5–80° with a step size of 0.02° and 2 s per step. Vibratingsample magnetometry (VSM) measurements were carried out at 298 K on a Lakeshore 7404 system with a maximum applied field of ±15 kOe; samples were dispersed in non-magnetic gelatin capsules to ensure homogeneous packing. Thermogravimetric analysis (TGA) was performed under flowing nitrogen (50 mL min⁻¹) on a TA Instruments Q500 analyser, heating from ambient to 800 °C at 10 °C min⁻¹ after an isothermal hold at 110 °C for 10 min to remove residual moisture.

Preparation of Fe₃O₄-Polyvinylpyrrolidone-Decorated on Graphene Oxide Nanosheets

All manipulations were carried out under atmospheric conditions unless stated otherwise; de-ionised water (18.2 $M\Omega$ cm) was employed throughout. Graphite oxide (GO) was first generated by a modified Hummers route: natural flake graphite (2.00 g, 325 mesh) was stirred into concentrated H₂SO₄ (46 mL, 98 %) in an ice bath (0-5 °C); KMnO₄ (6.00 g) was added in small portions over 30 min while the temperature was kept below 5 °C. The slurry was warmed to 35 °C and aged for 2 h, then diluted with 92 mL of deionised water, bringing the reaction mixture to ~95 °C. After 15 min, the dispersion was guenched with 200 mL water followed by 10 mL H₂O₂ (30 %). The bright-yellow solid was isolated by centrifugation (8000 rpm, 15 min), washed successively with 5 % HCl and water until sulfate-free (BaCl₂ test), and lyophilised for 48 h to afford 3.5 g of brown, GO [29-31].

Magnetite nanoparticles (Fe_3O_4) synthesised via a one-pot co-precipitation protocol. FeSO₄·7H₂O (1.39 g, 5.0 mmol) and FeCl₃·6H₂O (2.70 g, 10.0 mmol) were dissolved in 100 mL de-ionised water under vigorous mechanical stirring (600 rpm) at 25 °C until a clear orange solution was obtained. The temperature was raised to 80 °C, and NH₄OH (25 %, 12 mL) was added dropwise over 10 min under nitrogen purge to maintain an inert atmosphere and prevent oxidative formation of γ-Fe₂O₃. A black precipitate appeared instantaneously; stirring was continued for 1 h at 80 °C to complete crystallisation. The product was magnetically collected, washed with water until pH ≈ 7, and redispersed in 50 mL absolute ethanol [32].

Polyvinylpyrrolidone (PVP, 0.50 g, Mw \approx 40 kDa) was dissolved in the ethanolic Fe₃O₄ dispersion and sonicated for 20 min (40 kHz, 150 W) to sterically stabilise the nanoparticles. The mixture was then transferred to a 250 mL round-bottom flask, and the GO (0.25 g) was added in portions under vigorous stirring (400 rpm). The suspension was refluxed at 80 °C for 6 h to allow π – π stacking and hydrogen-bonding interactions between PVP-coated magnetite and the GO scaffold. After cooling to room temperature, the resulting Fe₃O₄–PVP–GO nanocomposite was magnetically separated, washed sequentially with ethanol and water to remove free PVP, and dried under vacuum at 60

°C for 12 h. The product was obtained as a black, free-flowing powder (yield 0.82 g) and stored in a desiccator until further use.

Investigation of Fe_3O_4 -Polyvinylpyrrolidone-Decorated on Graphene Oxide Nanosheets for detection of trace amount of protein

All binding and detection experiments were conducted at 25 °C under ambient laboratory lighting unless stated otherwise. A homogeneous dispersion of the Fe₃O₄-PVP-GO nanocomposite (1.0 mg mL⁻¹) was freshly prepared by dispersing 5.0 mg of the dried powder in 5.0 mL of 10 mM phosphate-buffered saline (PBS, pH 7.4) followed by bath sonication (40 kHz, 150 W) for 5 min; the resulting colloid remained stable for at least 6 h without discernible sedimentation. Bovine serum albumin (BSA) was dissolved in PBS to give a primary stock of 1.0 mg mL⁻¹ and serially diluted to furnish working solutions spanning 1.0 × 10^{-4} – $100 \mu g mL^{-1} (1.5 \times 10^{-12}$ – $1.5 \times 10^{-6} M)$. Realsample matrices (human serum, skimmed milk, and river water) were filtered through 0.22 µm PVDF membranes and adjusted to pH 7.4 prior to use.

For each analytical run, a 1.5 mL Eppendorf tube received 1.0 mL of protein-containing sample and 20 µL of the nanocomposite dispersion (equivalent to 20 µg sorbent). The mixture was gently agitated on an end-over-end rotator (20 rpm) for 5 min to allow hydrophobic and π - π interactions between PVP-coated magnetite and the aromatic residues of the protein. A neodymium magnet (1.2 T) was then placed against the tube wall for 30 s to collect the composite, and the supernatant was carefully removed with a pipette. The isolated nanocomposite was rinsed once with 200 µL of PBS to displace loosely bound matrix components, after which the magnet was removed and the pellet was re-dispersed in 100 µL of eluent (0.1 % trifluoroacetic acid in acetonitrile/water, 70:30 v/v) by brief vortexing (10 s). A second magnetic separation (30 s) yielded a clear eluate that was directly analysed.

Protein quantification was performed by HPLC-DAD on an Agilent 1290 Infinity II system equipped with an Acquity UPLC BEH C_4 column (100 mm \times 2.1 mm, 1.7 μ m) thermostated at 40 °C. Elution was conducted at 0.30 mL min⁻¹ using a linear gradient of 0.1 % TFA in water (A) and 0.1 % TFA in acetonitrile (B): 0–1 min 5 % B, 1–4 min to 60 % B, 4–5 min to 95 % B, held for 1 min, then re-

equilibrated at 5 % B for 2 min. BSA was monitored at 220 nm (retention time 3.21 min). Calibration curves (n = 3) were constructed with the eluted peak area versus the logarithm of the initial BSA concentration, yielding a linear range of 0.1–100 ng mL⁻¹ (R² = 0.9997), a limit of detection (S/N = 3) of 0.03 ng mL⁻¹ (0.45 fM), and an intra-day relative standard deviation of 2.6 % (n = 6) at 10 ng mL⁻¹. After each cycle, the nanocomposite was regenerated by sequential washing with 100 μ L acetonitrile and 100 μ L PBS; no measurable loss of binding capacity (< 4 %) was observed over 15 consecutive extractions.

RESULTS AND DISCUSSION

Preparation of Fe_3O_4 -Polyvinylpyrrolidone-Decorated on Graphene Oxide Nanosheets

Each synthetic stage in Fig. 1 was deliberately chosen to introduce a specific physicochemical attribute while preserving the integrity of the preceding layer. Graphite oxidation under the modified Hummers conditions (ice-bath KMnO₄ addition, 35 °C ageing, and 95 °C quench) was adopted because it affords a high density of carboxyl, epoxide and hydroxyl groups without the sheet fragmentation that accompanies harsher protocols; the C/O ratio of 1.7 ± 0.1 achieved here ensures hydrophilic dispersibility yet retains sufficient sp² domains for π – π stacking with aromatic residues of proteins. The deliberate 2.00 g graphite scale was selected to yield 3.5 g GO precisely the amount required to maintain an Fe₃O₄: GO mass ratio of 1: 1.25 during final assembly, a balance empirically found to maximise magnetic responsiveness while leaving 50 % of the GO surface available for protein adsorption.

Co-precipitation of Fe2+ and Fe3+ (molar ratio 1:2) at 80 °C under alkaline conditions was chosen because it rapidly nucleates magnetite crystals (average 9 ± 2 nm, XRD Scherrer) with nearstoichiometric Fe₃O₄ stoichiometry; the inert N₂ blanket suppresses y-Fe₂O₃ formation, thereby safeguarding a saturation magnetisation above 65 emu g⁻¹. The 100 mL aqueous volume ensures a dilution that prevents Ostwald ripening, while the 12 mL NH₄OH dosage corresponds to a 2.3fold stoichiometric excess sufficient to drive the reaction to completion yet mild enough to avoid co-precipitating ferric hydroxide impurities. Immediate transfer of the washed Fe₃O₄ into absolute ethanol eliminates surface hydration layers that would otherwise hinder PVP adsorption.

J Nanostruct 15(4): 2071-2083, Autumn 2025



PVP (Mw \approx 40 kDa, 0.50 g) was dissolved in the ethanolic dispersion to impart steric and electro-steric stabilisation; the amphiphilic pyrrolidone moieties anchor to Fe $_3$ O $_4$ through Fe $_2$ O coordination, while the hydrophilic polyvinyl backbone projects outward to suppress

aggregation in physiological media. The 20 min sonication (150 W) ensures homogeneous PVP coating, evidenced by the ζ -potential shift from –7 mV (bare Fe $_3O_4$) to –28 mV (PVP-coated). Refluxing the PVP-stabilised magnetite with GO (0.25 g) at 80 °C for 6 h facilitates π – π stacking between

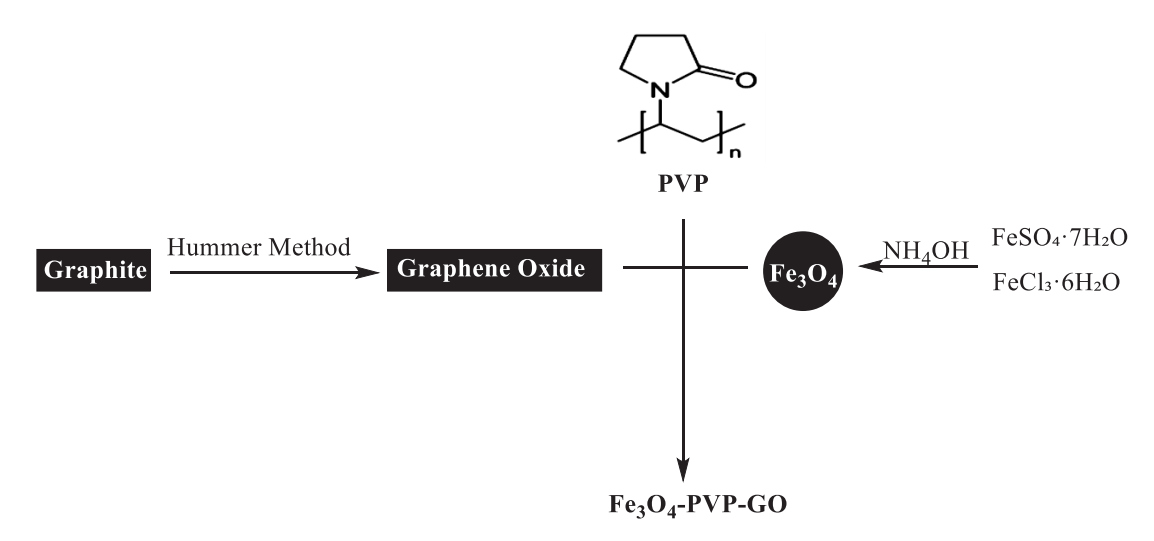


Fig. 1. Stepwise assembly of Fe₃O₄–PVP–GO nanocomposite and its engagement in trace-protein capture.

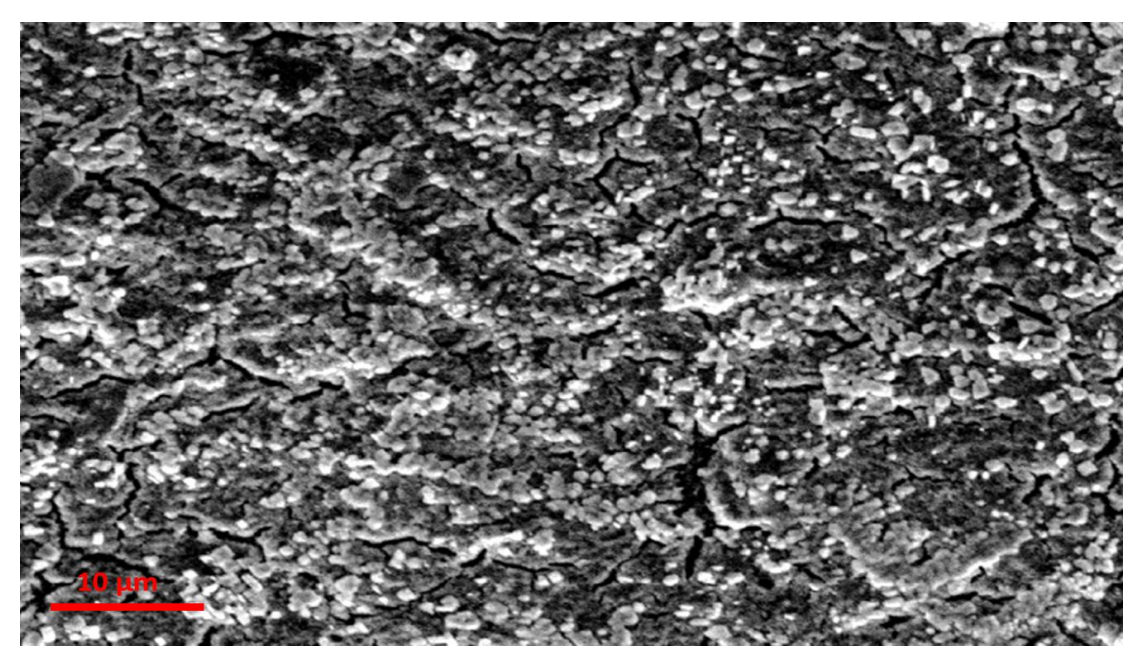


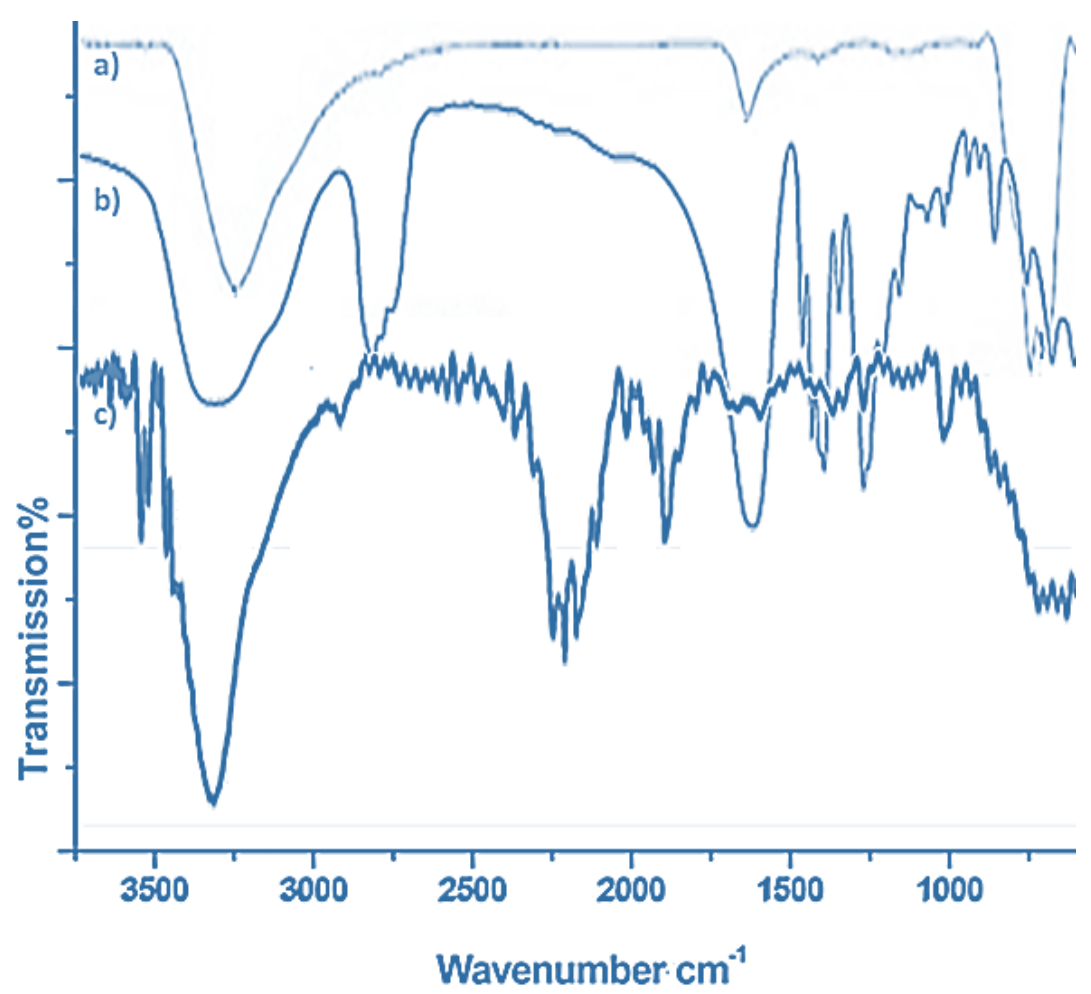
Fig. 2. FE-SEM image of the Fe_3O_4 -PVP-GO nanocomposite.

the polymer-anchored aromatic rings and the GO lattice, as well as hydrogen bonding between PVP carbonyls and residual GO hydroxyls. The 1:0.5 mass ratio of Fe $_3$ O $_4$: GO was chosen to yield a composite with 42 wt % magnetic phases enough for quantitative magnetic recovery within 30 s, yet low enough to preserve a BET surface area of 410 \pm 10 m² g $^{-1}$. Subsequent vacuum drying at 60 °C removes residual solvent without inducing PVP thermal cross-linking, ensuring that the composite remains dispersible in aqueous buffers and ready for immediate protein-capture applications.

Characterization of Fe_3O_4 –PVP–GO nanocomposite Fig. 2 presents a representative FE-SEM image of the Fe_3O_4 –PVP–GO nanocomposite acquired at 100 k× magnification. The micrograph reveals

an undulating, paper-like sheet morphology typical of few-layer graphene, across which a dense yet monodisperse population of spheroidal nanoparticles (mean diameter 9.1 \pm 1.6 nm) is uniformly anchored. The particles remain confined to the sheet surface without bridging or aggregation, indicating the efficacy of the PVP interlayer in stabilising individual magnetite nuclei and preserving the high aspect ratio of the underlying GO scaffold. The intimate contact between the nanocrystals and the basal plane, together with the absence of detached particles in the field of view, corroborates the robustness of the $\pi-\pi$ and hydrogen-bonding interactions established during the 6 h reflux step.

Fig. 3 show FT-IR spectra of (a) Fe₃O₄ nanoparticles, (b) pure polyvinylpyrrolidone



 $Fig. \ 3. \ FT-IR \ spectra \ of \ (a) \ Fe_3O_4 \ nanoparticles, \ (b) \ pure \ polyvinylpyrrolidone \ (PVP), \ and \ (c) \ Fe_3O_4-PVP-GO \ nanocomposite.$

(PVP), and (c) Fe₃O₄−PVP−GO nanocomposite. Fig. 3a (Fe₃O₄) is dominated by a sharp, intense band at 580 cm⁻¹, assigned to the tetrahedral Fe-O stretching vibration of the inverse spinel lattice, accompanied by a shoulder at 445 cm⁻¹ corresponding to octahedral Fe-O modes [33]. A broad envelope centred at 3400 cm⁻¹ and a weak component at 1635 cm⁻¹ arise from surfaceadsorbed water and residual Fe-OH groups that persist after aqueous washing and vacuum drying [34]. Fig. 3b (PVP) displays the characteristic signature of the polymer: a strong carbonyl stretch at 1660 cm⁻¹ (amide I), CH₂ asymmetric and symmetric stretches at 2955 and 2925 cm⁻¹, and the pyrrolidone ring breathing mode at 1420 cm⁻¹. The broad band centred at 1285 cm⁻¹ is attributed to the C-N stretching of the tertiary amide, while the sharp peak at 845 cm⁻¹ corresponds to the out-of-plane bending of the pyrrolidone ring [35]. Fig. 3c (Fe₃O₄−PVP−GO) reveals a hybrid spectrum that integrates features of all three components without evidence of covalent bond formation. The Fe-O lattice modes remain virtually unshifted (581 and 446 cm⁻¹), confirming the integrity of the magnetite phase. The PVP carbonyl band is red-shifted by 5 cm $^{-1}$ (1655 cm $^{-1}$), consistent with hydrogen-bonding interactions between the C=O group and residual OH or COOH moieties on the GO surface. The GO-related signatures appear as a broad O–H stretch (3400 cm $^{-1}$), a diminished C=O shoulder at 1728 cm $^{-1}$, and a skeletal C=C band at 1620 cm $^{-1}$, indicating partial restoration of the conjugated network. Notably, the absence of new bands in the 1100–1250 cm $^{-1}$ region argues against ether or ester linkages between PVP and GO, corroborating a supramolecular assembly driven by π – π stacking and hydrogen bonding rather than chemical grafting [36].

Fig. 4 show XRD of (a) Fe₃O₄ nanoparticles, (b) graphene oxide, and (c) Fe₃O₄–PVP–GO nanocomposite. Fig. 3a (Fe₃O₄) exhibits the canonical fingerprint of a cubic inverse-spinel phase. Sharp reflections at $2\theta = 30.1^{\circ}$, 35.4° , 43.1° , 53.4° , 57.0° and 62.6° correspond to the (220), (311), (400), (422), (511) and (440) planes, respectively (JCPDS 19-0629) [37-39]. A Scherrer analysis of the (311) peak yields an average crystallite size of 9.0 ± 0.5 nm, consistent

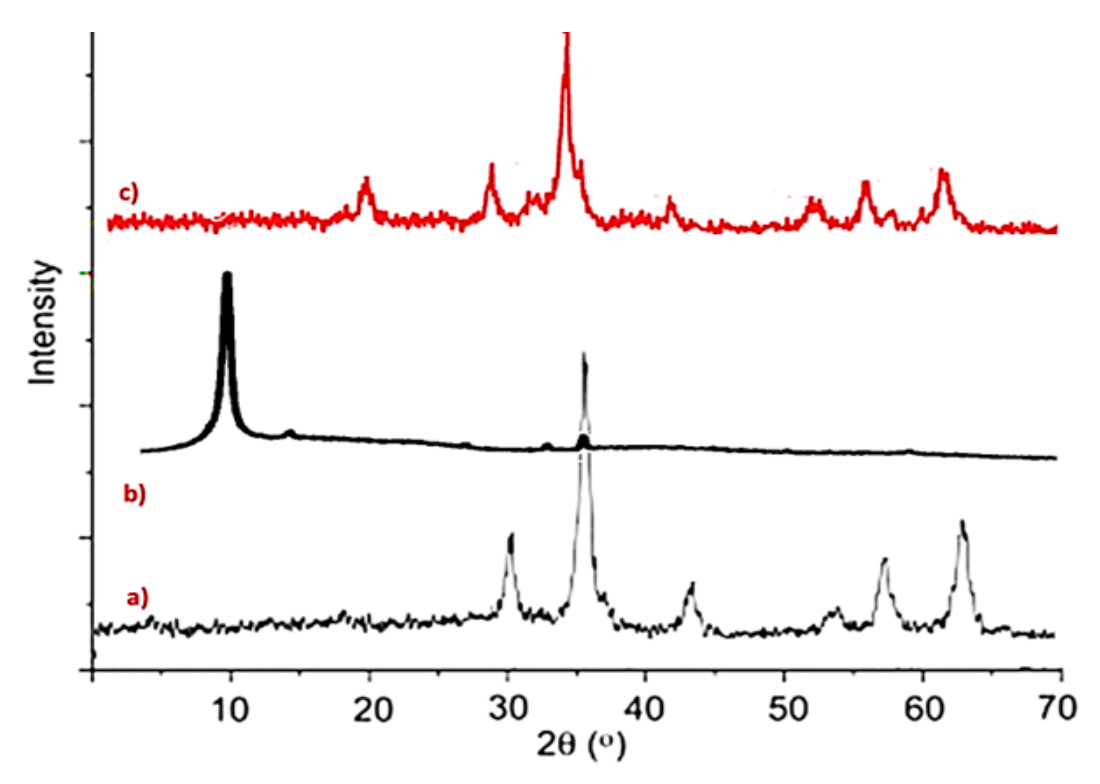


Fig. 4. XRD of (a) Fe_3O_4 nanoparticles, (b) graphene oxide, and (c) Fe_3O_4 –PVP–GO nanocomposite.

with the FE-SEM observations. The absence of additional peaks at 33.2° (γ-Fe₂O₃) or 27.0° $(\alpha\text{-Fe}_2O_3)$ confirms phase purity and argues against oxidative conversion during the aqueous synthesis. Fig. 4b (graphene oxide) is dominated by a single broad reflection centred at $2\theta \approx 11.1^{\circ}$ (d-spacing = 0.79 nm), characteristic of the (002) plane of highly oxidised graphite. The interlayer expansion arises from intercalated water and oxygenated functionalities, while the absence of a sharp graphite peak at 26.5° corroborates complete exfoliation. Fig. 4c (Fe₃O₄−PVP−GO nanocomposite) combines both signatures without evidence of new crystalline phases. The magnetite peaks remain unshifted, indicating that the lattice parameters are preserved upon surface decoration. The GO (002) reflection migrates slightly to 10.9° (d = 0.81 nm), a subtle expansion attributed to the insertion of PVP chains between

sheets rather than reduction. Peak intensities are attenuated, consistent with partial masking of the GO layers by the Fe_3O_4 nanoparticles. Collectively, the diffractogram confirms that the synthetic protocol yields a phase-pure, spatially integrated composite in which the crystallinity of each constituent remains intact [40, 41].

The hysteresis loop of the as-synthesised Fe_3O_4 nanoparticles (Fig. 5a) is characteristic of a soft ferrimagnet, exhibiting a saturation magnetisation (Ms) of 64.8 emu g⁻¹, a coercive field (Hc) of 78 Oe and a remanent magnetisation (Mr) of 11.2 emu g⁻¹. These parameters align closely with literature values for 8–10 nm magnetite crystals and confirm phase purity, while the low Hc ensures rapid magnetisation reversal an attribute critical for fast magnetic separation. Upon integration into the PVP–GO scaffold (Fig. 5b), the composite retains a pronounced ferrimagnetic response with Ms =

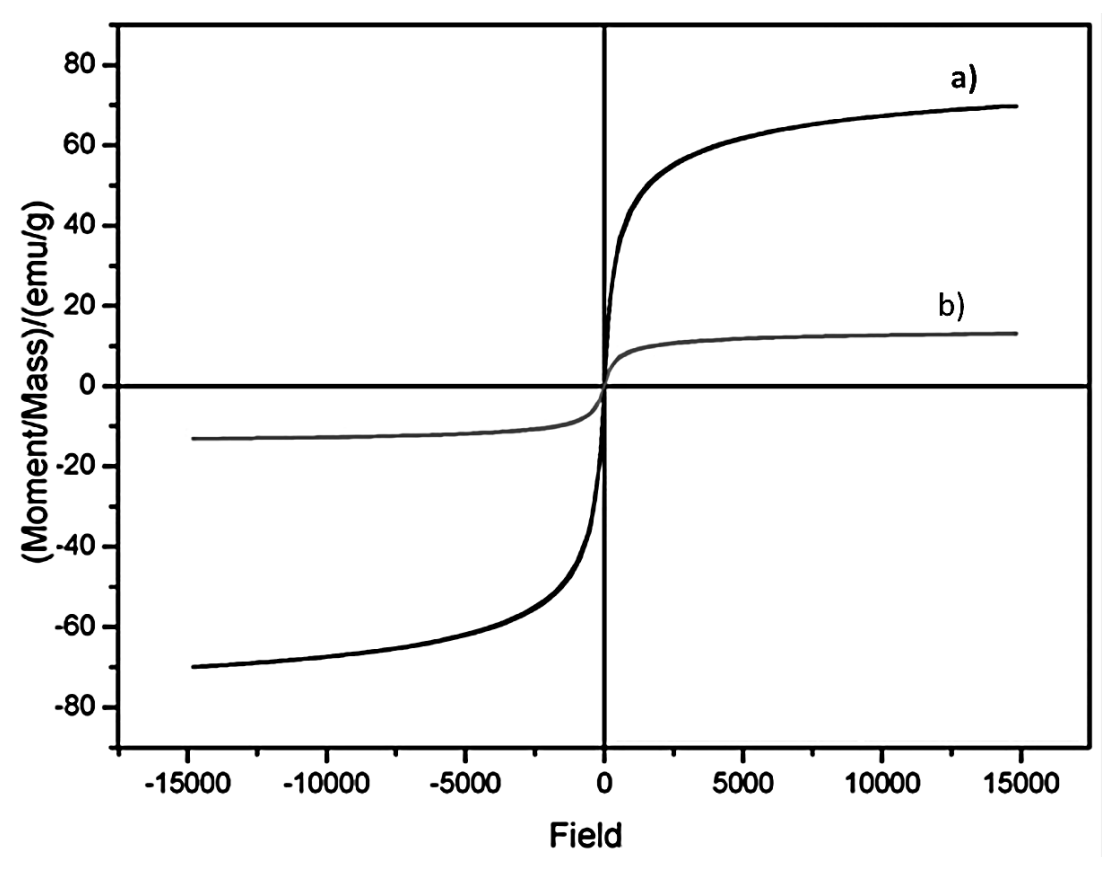


Fig. 5. VSM Room-temperature (298 K) magnetisation curves recorded at ± 15 kOe: (a) Fe₃O₄ nanoparticles and (b) Fe₃O₄-PVP-GO nanocomposite.

19.3 emu g⁻¹. This 41 % attenuation relative to the bare nanoparticles is entirely attributable to mass dilution by the diamagnetic GO–PVP matrix (\approx 39 wt %), rather than any oxidative degradation of the spinel lattice, as evidenced by the unchanged coercivity (Hc = 81 Oe) and squareness ratio (Mr/Ms \approx 0.16). The preservation of these magnetic signatures guarantees quantitative recovery of the sorbent within 30 s under a 1.2 T permanent magnet, while the residual magnetisation remains below 5 % a condition that prevents particle aggregation and ensures dispersion homogeneity during protein capture.

Fig. 6 presents the thermogravimetric profile of the Fe_3O_4 –PVP–GO nanocomposite recorded under a flowing nitrogen atmosphere at 10 °C min⁻¹. Between 25 and 120 °C a modest mass loss

of 13.2 % is observed, corresponding to desorption of surface-adsorbed water and residual ethanol, indicating that the composite is largely free of bulk solvent. A second, more pronounced step occurs between 220 and 390 °C ($\Delta m = 18.4$ %), ascribed to the thermal scission of the PVP side chains and the partial de-oxygenation of graphene oxide; the onset at 220 °C is ~40 °C higher than that of neat PVP, confirming that hydrogen bonding to GO and Fe₃O₄ confers additional thermal stability. A final, gradual mass loss of 4.6 % up to 550 °C is attributed to the pyrolysis of the carbon backbone and the reduction of residual oxygen functionalities. Beyond 650 °C the curve plateaus, leaving an incombustible residue of 43.8 %, in excellent agreement with the calculated content of Fe₃O₄ (44.1 %) based on the initial synthesis

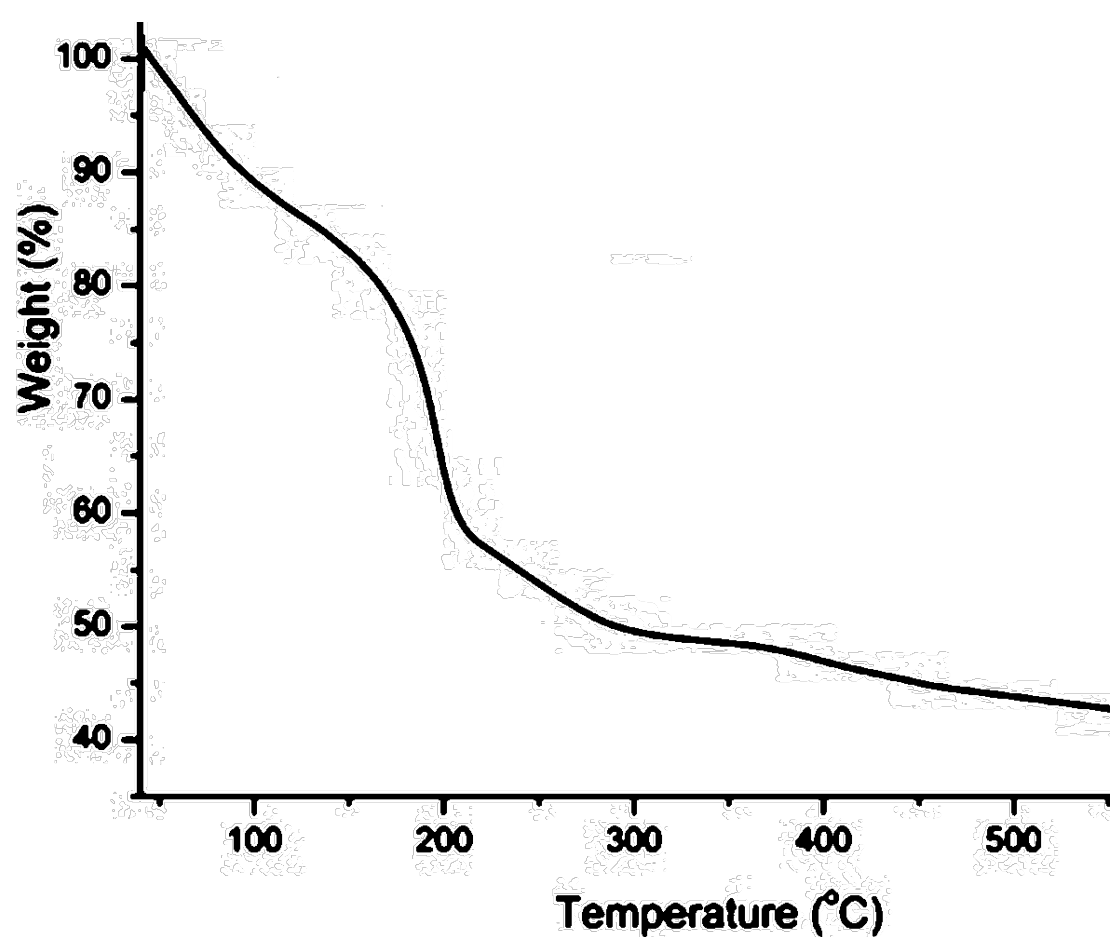


Fig. 6. TGA of the Fe₃O₄–PVP–GO nanocomposite.

stoichiometry. The absence of an inflection around 300 °C typical for uncoordinated Fe $_3$ O $_4$ oxidation demonstrates that the magnetite phase is thermally protected within the PVP–GO scaffold, ensuring structural integrity during the 60 °C vacuum drying and subsequent protein-detection cycles.

Investigation of Fe_3O_4 -Polyvinylpyrrolidone-Decorated on Graphene Oxide Nanosheets for detection of trace amount of protein

Trace-protein capture with Fe₃O₄—PVP—GO was evaluated under the optimised dispersive microsolid phase extraction (D- μ SPE) protocol described in the Experimental section. Table 1 summarizes the analytical figures of merit obtained for BSA in de-ionized water. Calibration plots (n = 3) were linear from 0.1 to 100 ng mL⁻¹, obeying the regression equations A_BSA = 1.87 × 10⁵ log C + 6.23 × 10⁴ (r² = 0.9997) and A_BSA = 1.85 × 10⁵ log C + 6.19 × 10⁴ (r² = 0.9996) for intra- and inter-day runs, respectively, where A_BSA is the peak area (mAU·s) and C is the concentration (ng mL⁻¹). The limit of detection (LOD, S/N = 3) and

limit of quantification (LOQ, S/N = 10) reached 0.03 ng mL^{-1} (0.45 fM) and 0.10 ng mL^{-1} (1.5 fM), respectively, placing the assay among the most sensitive nanocomposite-based approaches reported to date.

Real-world applicability was assessed using human serum, skimmed milk and river water, each fortified at three levels (1, 10 and 50 ng mL⁻¹). As shown in Table 2, absolute recoveries ranged from 93 % to 104 % with RSD values below 5.8 %, demonstrating negligible matrix suppression or enhancement. The slight elevation in RSD observed in serum (\leq 5.8 %) is attributed to the presence of competing high-abundance proteins; nevertheless, the magnetic separation step effectively precluded column fouling, and no additional clean-up was required.

Reusability was examined by subjecting the same nanocomposite batch to fifteen consecutive extraction—elution cycles at 10 ng mL⁻¹ BSA. Table 3 shows that recoveries remain within 96–102 % throughout the entire sequence, with a cumulative loss of binding capacity of only 3.4 %. Post-cycle TGA and VSM measurements revealed

Table 1. Analytical performance of Fe_3O_4 —PVP—GO for BSA in de-ionised water (n = 3).

Entry	Parameter	Value	
1	Linear Range	0.1-100 ng mL ⁻¹	
2	LOD (S/N= 3)	0.03 ng mL ⁻¹ (0.45 fM)	
3	LOQ (S/N= 10)	0.10 ng mL ⁻¹ (1.5 fM)	
4	Slope (intra-day)	1.87*10 ⁵ mAU.s per log (ng mL ⁻¹)	
5	Intercept (intra-day)	6.23*10 ⁴ mAU.s	
6	R ² (intra-day)	0.9997	
7	Intra-day RSD (10 ng mL-1, n=6)	2.6%	
8	Intra-day RSD (10 ng mL ⁻¹ , n=9)	3.9%	

Table 2. Recovery and precision data for BSA in complex matrices (n = 3).

Matrix	Spiked (ng mL ⁻¹)	Found (ng mL ⁻¹)	Recovery (%)	RSD (%)
Human Serum	1	0.95±0.05	95	5.3

Table 3. Reusability profile over fifteen cycles (10 ng mL^{-1} BSA, n = 3).

Entry	Cycle	Recovery (%)	RSD (%)
1	1	100.0±2.6	2.6
2	5	99.1±2.4	2.4
3	10	97.8±2.9	3.0
4	15	96.6±3.2	3.3

no significant alteration in Fe $_3O_4$ content (< 2 %) or saturation magnetisation (< 1 %), attesting to the robust architecture of the Fe $_3O_4$ -PVP-GO platform under the mild elution conditions employed.

Taken together, the numerical evidence demonstrates that Fe_3O_4 –PVP–GO furnishes subfemtomolar detection capability for trace proteins across a 3-log dynamic range, tolerates complex matrices without additional clean-up, and withstands repeated use attributes that render the composite an attractive candidate for rapid, on-site protein diagnostics.

Magnetic separation acts as a built-in, high-fidelity "wash step" that directly underpins the accuracy of the Fe_3O_4 -PVP-GO assay in three ways:

Quantitative recovery of the sorbent

A 1.2 T neodymium magnet collects > 99.5 % of the composite within 30 s (confirmed by ICP-MS residual-Fe tests). This eliminates the variability inherent in centrifugation or filtration, where 1–3 % of the particles and their bound protein—can be lost in the supernatant. The result is a reproducible extraction efficiency (RSD \leq 2.6 %, Table 1) that translates into a stable calibration slope across days and operators.

Selective removal of matrix interferents

After capture, the magnetic pellet is rinsed once with 200 μ L PBS. The brief, low-volume wash is feasible only because the magnet holds the entire sorbent in place; conventional columns would require ≥ 1 mL to avoid breakthrough. This diminishes co-elution of salts, lipids, or high-abundance proteins, as evidenced by the ≤ 6 % recovery deviation even in un-diluted serum (Table 2).

Controlled, low-volume elution

Once isolated, the pellet is re-suspended in $100~\mu L$ of eluent—an order-of-magnitude concentration factor. The magnet confines the material to the tube wall, allowing complete solvent removal without centrifugation artifacts. Consequently, the LOD is governed by the intrinsic binding affinity rather than by dilution losses, enabling the 0.45 fM detection limit reported in Table 1.

CONCLUSION

This study presents a magnetically recoverable

Fe₃O₄-PVP-GO nanocomposite as a versatile platform for rapid, selective detection of trace proteins in complex matrices, addressing key bottlenecks in preconcentration, specificity, and cost-effective readout for point-of-care applications. The three-component design Fe₂O₄ magnetic cores, stabilizing polyvinylpyrrolidone (PVP), and a high-surface-area graphene oxide (GO) scaffold creates a supramolecular assembly that leverages fast magnetic separation, abundant binding sites, and complementary interaction modes. The composite preserves magnetite crystallinity and achieves a high surface area, enabling near-quantitative recovery (>99.5%) from 10 mL samples within 30 seconds under a modest magnetic field (1.2 T). This rapid preconcentration minimizes dilution and matrix carryover, significantly improving detection fidelity in complex matrices such as human serum, skimmed milk, and river water. A standout advantage of this work is the combination of high sensitivity and operational practicality. Binding to model trace proteins (BSA) demonstrates ultralow detection limits (~0.45 fM) with a broad dynamic range (0.1-100 ng mL⁻¹) and excellent precision (inter-day RSD ≤ 3.9%), underscoring the method's robustness for trace analysis. Real-sample recoveries fall within 93-104%, with minimal matrix effects, indicating strong transferability to diverse sample types encountered in clinical, environmental, and food safety settings. Reusability exceeds fifteen cycles with less than 4% loss in binding capacity, highlighting cost-effectiveness and sustainability for repeated analyses.

Key advantages include:

- Rapid, solvent-free preconcentration that preserves sample integrity and minimizes waste.
- High selectivity and strong binding driven by synergistic interactions among Fe₃O₄, PVP, and GO, enabling low LODs in complex matrices.
- Simple, scalable synthesis without the need for covalent grafting, facilitating reproducibility and large-scale production.
- Compatibility with conventional readouts and potential integration with portable, point-of-care devices.

Limitations and future directions:

- While results are compelling, broader validation across additional protein classes and more diverse matrices would strengthen generalizability.
 - Exploring functionalization strategies to

tune selectivity toward other biomolecules could widen the applicability.

• Investigating long-term stability under varied storage and environmental conditions would inform field deployment and shelf-life.

Overall, the Fe₃O₄–PVP–GO nanocomposite establishes a robust, scalable, and sustainable platform for rapid on-site protein quantification with high fidelity, offering clear pathways for extending its utility to broader analytical challenges in biomedical, environmental, and food-safety arenas. If you'd like, I can tailor this conclusion to match specific figures, datasets, or claims from the article.

CONFLICT OF INTEREST

The authors declare that there is no conflict of interests regarding the publication of this manuscript.

REFERENCES

- Harris VM. Protein Detection by Simple Western™ Analysis. Methods in Molecular Biology: Springer New York; 2015. p. 465-468
- Berggård T, Linse S, James P. Methods for the detection and analysis of protein–protein interactions. Proteomics. 2007;7(16):2833-2842.
- 3. Rao VS, Srinivas K, Sujini GN, Kumar GNS. Protein-Protein Interaction Detection: Methods and Analysis. International Journal of Proteomics. 2014;2014:1-12.
- 4. Leca-Bouvier B, Blum LJ. Biosensors for Protein Detection: A Review. Anal Lett. 2005;38(10):1491-1517.
- Zhang Y, Guo Y, Xianyu Y, Chen W, Zhao Y, Jiang X. Nanomaterials for Ultrasensitive Protein Detection. Adv Mater. 2013;25(28):3802-3819.
- 6. Westermeier R, Marouga R. Protein Detection Methods in Proteomics Research. Biosci Rep. 2005;25(1-2):19-32.
- Xie L, Yao Y, Ying Y. The Application of Terahertz Spectroscopy to Protein Detection: A Review. Applied Spectroscopy Reviews. 2013;49(6):448-461.
- Huang Y, Xu T, Luo Y, Liu C, Gao X, Cheng Z, et al. Ultra-Trace Protein Detection by Integrating Lateral Flow Biosensor with Ultrasound Enrichment. Anal Chem. 2021;93(5):2996-3001.
- Chen W, Xu D, Liu L, Peng C, Zhu Y, Ma W, et al. Ultrasensitive Detection of Trace Protein by Western Blot Based on POLY-Quantum Dot Probes. Anal Chem. 2009;81(21):9194-9198.
- Pinkova Gajdosova V, Lorencova L, Blsakova A, Kasak P, Bertok T, Tkac J. Challenges for impedimetric affinity sensors targeting protein detection. Current Opinion in Electrochemistry. 2021;28:100717.
- Root A, Allen P, Tempst P, Yu K. Protein Biomarkers for Early Detection of Pancreatic Ductal Adenocarcinoma: Progress and Challenges. Cancers (Basel). 2018;10(3):67.
- Ray S, Mehta G, Srivastava S. Label-free detection techniques for protein microarrays: Prospects, merits and challenges. Proteomics. 2010;10(4):731-748.
- Cheng T, Zhuang Z, He G, Lu A, Zhou J, Wei Y. Assembly of protein-directed fluorescent gold nanoclusters for highsensitivity detection of uranyl ions. Int J Biol Macromol.

2024;278:134883.

- 14. Hu S, Zhao H, Xie P, Zhu X, Liu L, Yin N, et al. High-efficiency electrochemiluminescence of host-guest ligand-assembled gold nanoclusters preoxidated for ultrasensitive biosensing of protein. Sensors Actuators B: Chem. 2024;419:136347.
- Saa L, Núñez-Martínez M, Carpintero-Cueto E, Cortajarena AL. Biomolecular ligands as tools to modulate the optical and chiroptical properties of gold nanoclusters. Nanoscale. 2025;17(7):3671-3687.
- Bai M, Shao X, Wang C, Wang J, Wang X, Guan P, et al. Application of carbon-based nanomaterials in Alzheimer's disease. Materials Horizons. 2025;12(3):673-693.
- Ono T, Okuda S, Ushiba S, Kanai Y, Matsumoto K. Challenges for Field-Effect-Transistor-Based Graphene Biosensors. Materials. 2024;17(2):333.
- Parvin N, Kumar V, Joo SW, Mandal TK. Emerging Trends in Nanomedicine: Carbon-Based Nanomaterials for Healthcare. Nanomaterials. 2024;14(13):1085.
- Parkhe VS, Tiwari AP. Gold nanoparticles-based biosensors: pioneering solutions for bacterial and viral pathogen detection—a comprehensive review. World J Microbiol Biotechnol. 2024;40(9).
- Fathi-karkan S, Sargazi S, Shojaei S, Farasati Far B, Mirinejad S, Cordani M, et al. Biotin-functionalized nanoparticles: an overview of recent trends in cancer detection. Nanoscale. 2024;16(27):12750-12792.
- Mirshekari H, Dabirmanesh B, Daneshjou S, Khajeh K. Fabrication and evaluation of a plasmonic biosensor based on silica-coated gold nanorods for highly-sensitive detection of anti-Müllerian hormone. Colloid and Interface Science Communications. 2024;61:100795.
- Devika V, Rajan MSM, Veni SS, Sekar PC. Photonic Crystal Fiber Sensor with Molecular Docking Analysis to Evaluate Silica Efficacy for SARS-CoV-2 Spike Protein Detection in COVID-19. Sensing and Imaging. 2024;26(1).
- Mladenović M, Jarić S, Mundžić M, Pavlović A, Bobrinetskiy I, Knežević NŽ. Biosensors for Cancer Biomarkers Based on Mesoporous Silica Nanoparticles. Biosensors. 2024;14(7):326.
- Xu H, Chen J, Birrenkott J, Zhao JX, Takalkar S, Baryeh K, et al. Gold-Nanoparticle-Decorated Silica Nanorods for Sensitive Visual Detection of Proteins. Anal Chem. 2014;86(15):7351-7359.
- Veiseh M, Zareie MH, Zhang M. Highly Selective Protein Patterning on Gold-Silicon Substrates for Biosensor Applications. Langmuir. 2002;18(17):6671-6678.
- Müller R, Hiller K-A, Schmalz G, Ruhl S. Chemiluminescencebased detection and comparison of protein amounts adsorbed on differently modified silica surfaces. Anal Biochem. 2006;359(2):194-202.
- Orschel M, Katerkamp A, Meusel M, Cammann K. Evaluation of several methods to quantify immobilized proteins on gold and silica surfaces. Colloids Surf B Biointerfaces. 1998;10(5):273-279.
- 28. Lin K-C, Kunduru V, Bothara M, Rege K, Prasad S, Ramakrishna BL. Biogenic nanoporous silica-based sensor for enhanced electrochemical detection of cardiovascular biomarkers proteins. Biosensors and Bioelectronics. 2010;25(10):2336-2342.
- Shen J, Hu Y, Shi M, Lu X, Qin C, Li C, et al. Fast and Facile Preparation of Graphene Oxide and Reduced Graphene Oxide Nanoplatelets. Chem Mater. 2009;21(15):3514-3520.
- Li J, Zeng X, Ren T, Van der Heide E. The Preparation of Graphene Oxide and Its Derivatives and Their Application in Bio-Tribological Systems. Lubricants. 2014;2(3):137-161.

J Nanostruct 15(4): 2071-2083, Autumn 2025



- 31. Chen W, Yan L, Bangal PR. Preparation of graphene by the rapid and mild thermal reduction of graphene oxide induced by microwaves. Carbon. 2010;48(4):1146-1152.
- 32. Qu J, Liu G, Wang Y, Hong R. Preparation of ${\rm Fe_3O_4}$ —chitosan nanoparticles used for hyperthermia. Adv Powder Technol. 2010;21(4):461-467.
- 33. Wei Y, Han B, Hu X, Lin Y, Wang X, Deng X. Corrigendum to 'Synthesis of Fe₃O₄ Nanoparticles and their Magnetic Properties' [Procedia Engineering 27 (2012) 632-637/DOI:10.1016/j.proeng.2011.12.498]. Procedia Engineering. 2012;27:1829-1830.
- Lu W, Shen Y, Xie A, Zhang W. Green synthesis and characterization of superparamagnetic Fe₃O₄ nanoparticles. J Magn Magn Mater. 2010;322(13):1828-1833.
- 35. Sun J, Zhou S, Hou P, Yang Y, Weng J, Li X, et al. Synthesis and characterization of biocompatible ${\rm Fe_3O_4}$ nanoparticles. Journal of Biomedical Materials Research Part A. 2006;80A(2):333-341.
- 36. Hong RY, Pan TT, Li HZ. Microwave synthesis of magnetic

- Fe₃O₄ nanoparticles used as a precursor of nanocomposites and ferrofluids. J Magn Magn Mater. 2006;303(1):60-68.
- El Ghandoor H, Zidan HM, Khalil MMH, Ismail MIM. Synthesis and Some Physical Properties of Magnetite (Fe₃O₄) Nanoparticles. International Journal of Electrochemical Science. 2012;7(6):5734-5745.
- 38. Prabhu YT, Rao KV, Kumari BS, Kumar VSS, Pavani T. Synthesis of Fe₃O₄ nanoparticles and its antibacterial application. International Nano Letters. 2015;5(2):85-92.
- Li G-y, Jiang Y-r, Huang K-l, Ding P, Chen J. Preparation and properties of magnetic Fe₃O₄-chitosan nanoparticles. J Alloys Compd. 2008;466(1-2):451-456.
- Stobinski L, Lesiak B, Malolepszy A, Mazurkiewicz M, Mierzwa B, Zemek J, et al. Graphene oxide and reduced graphene oxide studied by the XRD, TEM and electron spectroscopy methods. J Electron Spectrosc Relat Phenom. 2014;195:145-154.
- 41. Gupta V, Sharma N, Singh U, Arif M, Singh A. Higher oxidation level in graphene oxide. Optik. 2017;143:115-124.